Self-consistent solutions for vacuum currents around a magnetic flux string

Hsiang-nan Li, David A. Coker, and Alfred S. Goldhaber
Institute for Theoretical Physics, State University of New York, Stony Brook, New York 11794-3840
(Received 29 June 1992)

We consider the feedback effects of the vacuum currents induced by a magnetic flux string in $2+1$ dimensions. Self-consistent induced charge and current densities that satisfy both the Dirac and Maxwell equations are given for the dimensionless coupling constant $g \equiv e^2/m \to 0$ and $g \to \infty$. These quantities for arbitrary g are inferred from the results of the two limiting cases, and also studied numerically.

PACS number(s): 12.20.Ds

I. INTRODUCTION

The presence of a classical background gauge field (BGF) for QED in $2+1$ dimensions has been shown to polarize the Dirac sea, giving rise to induced charge and current densities [1–6]. This intriguing phenomenon has been widely studied to lowest order in $g \equiv e^2/m$ ($e<0$ and m being the fermion charge and mass, respectively), and some important conclusions are established. The total induced charge Q is found to be a topological invariant proportional to the spectral asymmetry of the Dirac operator $Q=-eF/2$, with F the total magnetic flux, $0 \le F \le 1$ [1,5,6]. For a spatially uniform BGF, the feedback interactions of the vacuum currents are manifested by an effective photon mass $e^2/4\pi$ [2,7,8].

The particular system with a magnetic flux string (MFS) located at the origin has been investigated to order g in detail [5,6]. It is shown that both the induced charge and current densities, obtained by summing up contributions from all fermion partial waves, exhibit singularities at the origin and decay exponentially at large radius r with a characteristic length scale $1/m$, the fermion Compton wavelength. The total charge is computed and the relation $Q=-eF/2$ is verified. The induced current produces a return flux of order g opposing the applied one. In particular, as $F \to 1$, a charge $-e/2$ is attracted to the MFS, which can be understood as due to the existence of a highly singular bound state located at the origin.

However, the above conclusions, drawn without including feedback interactions whose importance is proportional to the magnitude of g, are only valid in the limit $g \ll 1$. For larger g the lowest-order behavior of the vacuum currents is expected to be modified by feedback effects [5]. The quantity e^2/m is equivalent to the ratio of the fermion Compton wavelength to the photon one. All significant variation of the vacuum polarization is confined to a region on the order to the photon wavelength, since the exchanged massive photon can only propagate on this length scale. For vanishing g, the photon wavelength is so large that the induced charge and current can be distributed in a region characterized by the fermion Compton wavelength, as shown in the previous approaches [5,6]. At the same time, a negative induced charge $eF/2$ and a reverse induced current, required by conservation laws, are located at infinity. These distributions will not be changed dramatically until the photon wavelength comes close to the fermion one.

When the photon wavelength is smaller than the fermion Compton wavelength ($g>1$), feedback interactions become more influential, and the lowest-order results cannot give an appropriate description for the system. In this case one expects that the opposite vacuum currents located at infinity will move toward the origin and cancel the positive ones near the MFS. The resulting distribution is then restricted to a region characterized by the photon wavelength. A full understanding of this transition of length scales due to feedback effects requires an all-order consideration.

Our aim in this paper is to give a full picture for the vacuum polarization in the presence of the MFS. This system is described by $(2+1)$-dimensional Dirac and Maxwell equations coupled together through feedback interactions. The former generates vacuum currents governed by the combination of the applied and induced potentials, while the latter produces the induced scalar and vector potentials from the vacuum currents. We shall derive self-consistent solutions for these quantities that satisfy both of the above equations in the limits $g \to 0$ and $g \to \infty$ explicitly. The results lead to a rough sketch for the case of arbitrary g.

Our conclusion is that when g is large enough the induced charge and current densities contract to the origin with shrinking photon wavelength. The total induced charge near the origin is less than the lowest-order result, $-eF/2$, and approaches zero with increasing g. The total induced flux opposes the applied one and its magnitude approaches F. As $g \to \infty$, the photon wavelength is so small that all the opposite vacuum currents move toward the origin and the cancellations become complete. The MFS becomes completely invisible.

Note that the induced gauge fields in our analysis are still treated as classical quantities, and quantum fluctuations associated with them are ignored. Thus, our approach can be thought of as a mean-field approximation. This approximation will become exact as $g \to \infty$ because virtual photons are so massive in this limit that the quantum fluctuations die out completely. The virtual fermion-antifermion pairs that give rise to the phenomenon of vacuum polarization interact only with

an induced BGF without radiative corrections. Based on this argument, our calculation for large g makes sense.

A difference in the amount of induced charge for the two cases $m=0$ and $m\to 0$ has been proposed in Refs. [8,9]. It is found that setting $m=0$ at the outset leads to a vanishing induced charge density $\rho(r)$ and thus zero total charge, while the topological invariant $Q=-(eF/2)\mathrm{sgn}(m)$, independent of $|m|$, is not altered if we take the limit $m\to 0$. It is further argued that this amount of induced charge is distributed at infinity, since $\rho(r)$ diminishes at any finite r as $m\to 0$. We shall point out that this difference disappears in an all-order consideration because both cases lead to a vanishing induced charge corresponding to the $g\to\infty$ limit.

The calculation involved in the case $g\to 0$ is simple [5,6]. The fermion wave functions are obtained by solving the Dirac equation directly without the induced scalar and vector potentials. The induced charge and current densities, computed from these wave functions, are self-consistent because feedback interactions are negligible. For larger g, the exact calculation is extremely difficult. Therefore, some approximations will be made in the intermediate stage. We shall ignore the induced scalar potential at first and absorb the induced vector potential into a radius-dependent effective flux. The complexity of the formula relating the wave functions to the induced current density is then greatly reduced. Then we solve this equation along with the Maxwell one numerically. The expected features of the vacuum currents are observed. We show that the approximations turn out to be exact as $g\to\infty$, and the above solutions become self-consistent in this limit.

The rest of this paper is organized as follows. The results for $g\to 0$ are reviewed in Sec. II. Some useful formulas which will be employed later are given. The opposite induced charge is explicitly shown to be distributed at infinity. In Sec. III we obtain the self-consistent solutions for the induced currents and potentials for $g\to\infty$. The approximations mentioned above are used. A model form for the induced vector potential is proposed. In Sec. IV the case of intermediate g is studied, and the accuracy of the approximations is explored numerically. Section V gives conclusions.

II. PREVIOUS RESULTS ($g\ll 1$)

In this section we explicitly define the system described by the $(2+1)$-dimensional Dirac equation in the presence of the MFS [5,6]. Results are given for the induced charge and current densities when feedback effects are ignored. This is equivalent to analyzing the system in the $g\ll 1$ limit. The formalism presented here also will be useful for the case $g\gg 1$.

The complete Dirac Hamiltonian for $(2+1)$-dimensional QED is given by

$$H=\boldsymbol{\alpha}\cdot(\mathbf{p}-e\,\mathbf{A}_{\mathrm{app}}-e\,\mathbf{A})+\beta m+eA_0\ , \tag{1}$$

where the representation $\boldsymbol{\alpha}=(\sigma_1,\sigma_2)$, $\beta=\sigma_3$ is used, σ_1, σ_2, and σ_3 being the Pauli matrices [3,10]. The term $\mathbf{A}$ is the induced vector potential derived from the induced current density. The induced scalar potential A_0 is defined similarly. The applied vector potential $\mathbf{A}_{\mathrm{app}}$ due to the MFS is described in cylindrical coordinates by [3,5]

$$e\,\mathbf{A}_{\mathrm{app}}=\frac{F}{r}\hat{\theta} \tag{2}$$

with $F\equiv(e/2\pi)\oint\mathbf{A}_{\mathrm{app}}\cdot\mathbf{d}l$ the total magnetic flux.

Now we review previous results where the feedback effects on $\mathbf{A}$ and A_0 initially are ignored. The two-component eigenstates of energy and angular momentum for the Dirac Hamiltonian are proposed to have the general form

$$\psi_{kn}(r,\theta)=\begin{bmatrix}\chi_1(r)\\ \chi_2(r)e^{i\theta}\end{bmatrix}e^{in\theta}\ ,$$

where the functions $\chi_1(r)$ and $\chi_2(r)$ satisfy the set of equations

$$\begin{aligned}(E-m)\chi_1&=-i\left[\frac{d}{dr}\chi_2+\frac{\nu+1}{r}\chi_2\right]\ ,\\ (E+m)\chi_2&=-i\left[\frac{d}{dr}\chi_1-\frac{\nu}{r}\chi_1\right]\ .\end{aligned} \tag{3}$$

The normalized solutions to Eq. (3) are simply [5,6]

$$\psi_{k\nu}(r,\theta)=e^{in\theta}\left[\frac{k}{4\pi}\frac{E+m}{E}\right]^{1/2}\begin{bmatrix}J_{q\nu}(kr)\\ \dfrac{iqk}{E+m}J_{q(\nu+1)}(kr)e^{i\theta}\end{bmatrix}\ , \tag{4}$$

with

$$\begin{aligned}&n\in N\ ,\quad \nu\equiv n-F\ ,\quad 0<F<1\ ,\\ &0\le k\le\infty\ ,\quad E=\pm\sqrt{k^2+m^2}\ ,\\ &q=\begin{cases}+1\ , & n\ge 0\ ,\\ -1\ , & n<0\ ,\end{cases}\end{aligned} \tag{5}$$

with q chosen to make $\psi_{k\nu}$ square integrable at the origin.

The induced vacuum currents are expressed as a sum over all products of partial waves [1]:

$$e\langle j^\mu\rangle=\frac{-e}{2}\sum_{k,\nu}\mathrm{sgn}(E_k)\bar{\psi}_{k\nu}\gamma^\mu\psi_{k\nu}\ , \tag{6}$$

where appropriate regularization is assumed [11,12]. The terms in Eq. (6) corresponding to high angular momentum, or large ν, do not contribute due to regularization, and the expression is simplified using Wick rotation to give [6]

$$\begin{aligned}\rho(r)&\equiv e\langle j^0\rangle\\ &=-em\frac{\sin(\pi F)}{\pi^3}\int_m^\infty dk\frac{k}{\sqrt{k^2-m^2}}K_F^2(kr)\ ,\end{aligned} \tag{7}$$

for the induced charge density and

$$j(r)\equiv e\langle j^{\theta}\rangle = e\frac{\sin(\pi F)}{\pi^3}\int_m^{\infty} dk \frac{k}{\sqrt{k^2-m^2}}[K_F^2(kr)-K_{F-1}(kr)K_{F+1}(kr)] \tag{8}$$

for the induced current density. $K_F(kr)$ is the modified K-Bessel function of order F. The formula for the charge density $\rho(r)$ is obtained by Wick rotating the integral [which contains only two terms $J_F^2(kr)$ and $J_{-F}^2(kr)$ after a symmetric cancellation in the sum] to the imaginary axis in the complex k plane. In the derivation of the current density $j(r)$, a similar cancellation is achieved using the single recursion relation [6]

$$\nu J_{\nu}(x)=\frac{x}{2}[J_{\nu-1}(x)+J_{\nu+1}(x)] . \tag{9}$$

The radial current density $\langle j^r\rangle$ vanishes due to the rotational and time translational symmetries of the system. The integrals in Eqs. (7) and (8) can be performed explicitly for $F=\frac{1}{2}$ with the results [5,6]

$$\rho(r)=\frac{-me}{2\pi^2 r}K_0(2mr) ,$$
$$j(r)=\frac{-me}{2\pi^2 r}K_1(2mr) . \tag{10}$$

The general features of the induced charge and current densities are summarized as follows. Both of them diverge near the origin and decay exponentially at large r with a length scale $1/m$. The total induced charge is easily computed to be $Q=-eF/2$ by integrating Eq. (7) over all space. As F approaches 1 from 0, $\rho(r)$ increases with F for all r when $F<\frac{1}{2}$, and then decreases at large r and increases at small r when $F>\frac{1}{2}$. Therefore, the charge becomes localized toward the MFS as $F\to 1$. For $F=1$, a charge of $-e/2$ is concentrated at the origin. Of course in a self-consistent solution, an extremely localized charge does not exist due to strong repulsion. The behavior of $j(r)$ is similar to that of $\rho(r)$ for $0<F<\frac{1}{2}$, but it decreases for all r for $F>\frac{1}{2}$. There is no localization of current as $F\to 1$. For $F=1$ the current disappears.

The induced current gives rise to a magnetic field which in turn defines an induced flux, F_I. This induced return flux cancels part of the applied flux from the MFS as seen from the result [6]

$$F_I=\frac{-g}{12\pi}F(1-F^2) \quad (0\le F\le 1) . \tag{11}$$

The induced flux and thus the feedback effects are of order g, which vanishes as $g\to 0$. Equations (7), (8), and the induced scalar and vector potentials derived from them constitute the self-consistent solutions in this case.

Now we shall show explicitly that a negative induced charge $eF/2$ is located at infinity. This charge, coming from the partial waves with high angular momenta, does not appear in the calculation due to regularization. In fact, the calculation for $\rho(r)$ does not involve regularization as shown in the expression

$$\rho(r)=-\frac{me}{4\pi}\sum_{n=-\infty}^{\infty}\int_0^{\infty} dk \frac{k}{\sqrt{k^2+m^2}}[J^2_{q(n-F)}(kr)-J^2_{q(n-F+1)}(kr)] , \tag{12}$$

which follows the definition of the current density equation (6) and the lowest-order solutions equation (4). No regularization is assumed because the k integrals are now well defined in spite of the divergence of the single integral

$$\int_0^{\infty} dk \frac{k}{\sqrt{k^2+m^2}}J_{\nu}^2(kr) .$$

After the symmetric cancellation we have

$$\rho(r)=\rho_0(r)+\lim_{n\to\infty}\rho_n(r) , \tag{13}$$

where

$$\rho_0(r)=-\frac{me}{4\pi}\int_0^{\infty} dk \frac{k}{\sqrt{k^2+m^2}}[J^2_{-F}(kr)-J_F^2(kr)] ,$$
$$\rho_n(r)=\frac{me}{4\pi}\int_0^{\infty} dk \frac{k}{\sqrt{k^2+m^2}}[J^2_{n-F}(kr) - J^2_{n+F}(kr)] . \tag{14}$$

Note that we do not take n to ∞ until ρ_n is integrated over r. Integration of $\rho_0(r)$ over all space gives the standard results $Q=-eF/2$. A straightforward calculation indicates that an induced charge $eF/2$, which is independent of n, is derived from the second term $\rho_n(r)$. This opposite charge is distributed at infinity since $\rho_n\sim 1/n \to 0$ at finite r as $n\to\infty$. If regularization is introduced, however, it will disappear when n approaches ∞. We shall show in the next section that the opposite induced charge moves toward the origin as g increases.

III. LARGE-g LIMIT

When the coupling constant g increases, feedback effects become important. The scalar and vector potentials created by the induced charge and current densities affect the motion of the fermions. The change in the behavior of the fermions in turn affects the induced charge and current distributions. Therefore, it is necessary to take into account this interplay in order to have a consistent picture for the system. Including influences of the induced scalar and vector potentials simultaneously will make the situation too difficult to handle. Our first at-

tempt is to ignore the scalar potential and obtain a consistent solution for the induced current density that satisfies both the Dirac and Maxwell equations. This study, though not complete, might give a hint about the vacuum polarization in the limit $g \to \infty$.

If we make the variable changes $E \to mE$, $r \to r/m$, and $\mathbf{A} \to -e\mathbf{A}$ in Eq. (3), the Dirac equations without the induced scalar potential A_0 are written in terms of dimensionless quantities as

$$(E-1)\chi_1(r) = -i\left[\frac{d}{dr}\chi_2(r) + \frac{\nu+1}{r}\chi_2(r) + gA(r)\chi_2(r)\right], \tag{15}$$

$$(E+1)\chi_2(r) = -i\left[\frac{d}{dr}\chi_1(r) - \frac{\nu}{r}\chi_1(r) - gA(r)\chi_1(r)\right],$$

where $g = e^2/m$ is shown explicitly in order to indicate the feedback interactions. The induced vector field $A(r)$ obeys the Maxwell equation

$$\frac{d}{dr}\left[\frac{1}{r}\frac{d}{dr}(rA)\right] = -4\pi j(r), \tag{16}$$

or the equivalent integral form

$$rA(r) = 2\pi\left[\int_0^r dr' r'^2 j(r') + r^2\int_r^\infty dr' j(r')\right], \tag{17}$$

where the induced current density $j(r)$ is calculated from the solutions χ_1 and χ_2 to Eq. (15). A direct numerical approach for solving Eqs. (15) and (16) has been attempted. However, it is found that the results are sensitive to the cutoff in the k integral, and that the convergence of the sum over partial waves is very slow. Therefore, an exact numerical solution seems not practical, and we resort to an analytic approach.

Our first step is to find approximate solutions to Eq. (15) which avoid the difficulties encountered in the numerical study. A reasonable candidate that takes into account the effect of the induced vector potential and maintains the simplicity of analysis is

$$\psi_{k\nu}(r,\theta) = e^{in\theta}\left[\frac{k}{4\pi}\frac{E+1}{E}\right]^{1/2}\begin{bmatrix} J_{q[\nu+grA(r)]}(kr) \\ \dfrac{iqk}{E+1}J_{q[\nu+1+grA(r)]}(kr)e^{i\theta}\end{bmatrix}. \tag{18}$$

Note that the index ν of the Bessel function has been replaced by the function $\nu+grA(r)$. If Eq. (18) is inserted into Eq. (15), all the terms cancel except those due to the derivative of the indices of the Bessel functions, or the derivative of the induced vector potential $gd(rA)/dr$. The approximation will be good if this quantity is small. We shall observe that as $g \to \infty$, Eq. (18) turns out to be exact. The motivation for this approximation is that the induced vector potential decreases the applied one by different amounts at different r, and the resulting combination is absorbed into radius-dependent indices of the wave functions.

In this approximation $j(r)$ maintains a similar expression to Eq. (8), with the magnetic flux F replaced by the factor $F - grA(r)$. Applying the same recursion relation Eq. (9), we derive the formula for the induced current density:

$$j(r) = \frac{\sin[(F-grA(r))\pi]r}{\pi^3}\int_1^\infty dk \frac{k^3}{\sqrt{k^2-1}}\left[K_{F-grA(r)-1}(kr)K_{F-grA(r)+1}(kr) - K^2_{F-grA(r)}(kr)\right]. \tag{19}$$

Our aim is to solve Eqs. (16) and (19) for a consistent induced vector potential $A(r)$. A careful observation of Eq. (17) shows that, if $r^2 j(r)$ is finite at the origin and vanishes fast enough at infinity, $rA(r)$ approaches zero as $r \to 0$ and a constant h as $r \to \infty$. Substituting these qualitative properties of $rA(r)$ into Eq. (19), the assumed behavior of $r^2 j(r)$ described above is maintained. Therefore, a consistent description for the system should contain these features.

Evaluating Eq. (19) with the assumed property of $rA(r)$ inserted, we have the following boundary conditions for the induced current density:

$$r^2 j(r) \sim \frac{1}{4\pi}\left[\frac{1}{4} - F^2\right]\tan(F\pi), \quad r \to 0,$$
$$j(r) \sim \frac{1}{4\pi^{3/2}}\frac{\exp(-2r)}{r^{3/2}}\sin[(F-gh)\pi], \quad r \to \infty. \tag{20}$$

In turn, from Eqs. (16) and (20), $rA(r)$ behaves as

$$rA(r) \sim \text{const} \times r, \quad r \to 0,$$
$$rA(r) \sim h\left[1 - \frac{\exp(-2r)}{\text{const} \times r^{1/2}}\right], \quad r \to \infty. \tag{21}$$

A numerical analysis using an iterative method (described in Sec. IV) reveals that as g increases the constant h decreases, and the slope s to reach this height increases. However, the convergence of the numerical solution becomes very slow for large g. Because h and s are the important parameters that characterize the behavior of the induced vector potential, we propose a model form for $rA(r)$ with these two parameters, which are determined by the boundary conditions at the origin and infinity. Once the parameters are fixed, the behavior of the induced vector potential in the limit $g \to \infty$ can be studied analytically. The accuracy of the model function will be justified in Sec. IV. A possible model for $rA(r)$ that satisfies the requirements of Eq. (21) is given by

$$rA(r)=h\left[1-\frac{\exp(-2r)}{\exp(-sr^{1/2})+sr^{1/2}}\right] . \tag{22}$$

Examining Eq. (22), we find that $rA(r)$ possesses the limiting expressions

$$\begin{aligned} rA(r)&\sim h\left[2+\frac{s^2}{2}\right]r , \quad r\to 0 , \\ rA(r)&\sim h\left[1-\frac{\exp(-2r)}{sr^{1/2}}\right] , \quad r\to\infty , \end{aligned} \tag{23}$$

which exhibit the required behavior of Eq. (21). The physical meaning of h and s can be understood as follows. The product gh is exactly the total induced magnetic flux, and s defines the characteristic length scale $r\sim 1/s^2$, over which the induced current is distributed. Thus, the dependence on s in the $g\to\infty$ limit can verify our statement proposed in the Introduction. Inserting Eqs. (20) and (23) into (16) we obtain a set of coupled equations for h and s:

$$\begin{aligned} h\left[2+\frac{s^2}{2}\right]&=\left[\frac{1}{4}-F^2\right]\tan(F\pi) , \\ \frac{h}{s}&=\frac{\sin[(F-gh)\pi]}{4\sqrt{\pi}} . \end{aligned} \tag{24}$$

Equation (24) can be solved simply, and the g dependence of h and s is shown in Fig. 1, from which we find, in the $g\to\infty$ limit,

$$h\sim\frac{F}{g} , \quad s\sim\left[\frac{2g}{F}\right]^{1/2}\left[\left[\frac{1}{4}-F^2\right]\tan(F\pi)\right]^{1/2} . \tag{25}$$

It is evident from Eq. (25) that for large g the induced magnetic flux almost cancels the applied one due to the MFS, and thus makes $j(r)$ vanish everywhere except the tiny region characterized by $r\sim 1/s^2\sim 1/g$, or the photon wavelength in our present notation. The small $j(r)$ in turn defines a small induced vector potential $A(r)$ signified by h. However, the induced feedback integration $gA(r)$ is strong enough to cancel the applied one.

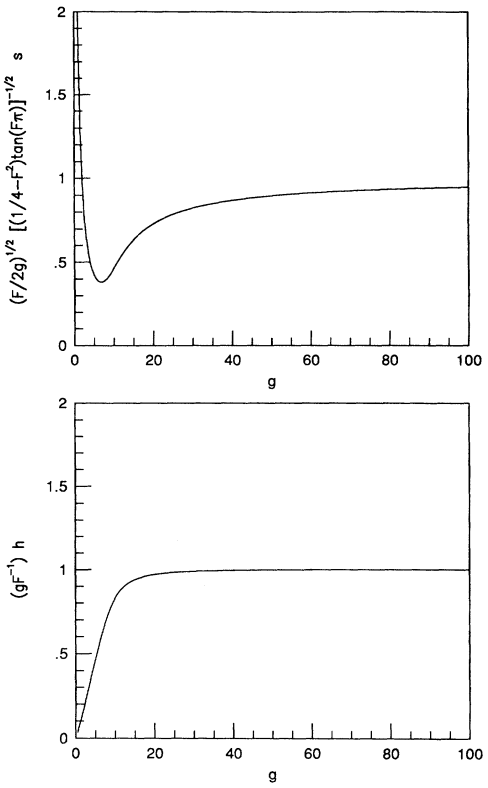

FIG. 1. The g dependence of parameters h and s.

Using an expression for the charge density similar to Eq. (19),

$$\rho(r)=\frac{\sin[(F-grA(r))\pi]}{\pi^3}\int_1^\infty dk\frac{k}{\sqrt{k^2-1}}K^2_{F-grA(r)}(kr) , \tag{26}$$

it is found that $\rho(r)$ vanishes for $r>0$, and the total induced charge $Q=(F-gh)/2\sim 0$ for $g\gg 1$ because $rA(r)=h$ is a constant in this limit. This result is consistent with the conclusion that Q is a topological invariant proportional to the total magnetic flux $F-F_I$, $F_I=gh$. From Eqs. (24) and (25) we find

$$Q=\frac{F-gh}{2}=\left[\frac{2}{\pi}\right]^{1/2}\left[\frac{F}{g}\right]^{3/2}\left[\left[\frac{1}{4}-F^2\right]\tan(F\pi)\right]^{1/2}[1+\mathcal{O}(1/g^3)] . \tag{27}$$

These observations indicate that the negative vacuum currents located at infinity move toward the origin and cancel the positive ones. Note that Q decreases as $1/g^{3/2}$, and thus the effect of the induced scalar potential gA_0 is suppressed by $1/g^{1/2}$. The neglect of A_0 at the outset is justified for large g. The approximate wave functions in Eq. (18) become exact because $grA(r)$ is essentially constant as $g\to\infty$. The derivation from the exact solutions appears only in the small range $r\lesssim 1/g$, and also vanishes with large g. Based on the above justifications we obtain a self-consistent picture for the system when $g\to\infty$ as follows. All the induced quantities $j(r)$, $\rho(r)$, $A(r)$, and $A_0(r)$ vanish. The feedback interaction $gA(r)$ is large enough to cancel the applied vector potential, but $gA_0(r)$ is still small. This leaves no contradiction to the vanishing of $j(r)$ and $\rho(r)$.

From the consistent solutions for $g\to 0$ and $g\to\infty$ derived above, it is easy to determine how the vacuum

currents are distributed for arbitrary g. For vanishing g, the induced negative charge $eF/2$ is located at infinity, and the positive one $-eF/2$ is distributed near the origin with an exponentially decaying tail. As g increases, the negative charge begins to move toward the origin to cancel part of the positive one and compress the distribution into a region characterized by $1/g$. When $g \gg 1$, the cancellation becomes complete and the space is left unpolarized. The description for the induced current density is similar.

Our results also solve the apparent contradiction between the two cases $m=0$ and $m \to 0$ mentioned in the Introduction. From the all-order investigation in this section, both analyses imply vanishing total induced charge corresponding to the limit $g \to \infty$, and the contradiction disappears.

IV. INTERMEDIATE g

As mentioned in Sec. III, a direct numerical analysis for the coupled integral equations (17) and (19) is very difficult due to the slow convergence of $A(r)$ as $g \to \infty$. Therefore, we proposed a model form for $rA(r)$ in order to study analytically the behavior of the induced vector potential for large g. For intermediate values of g, however, explicit numerical solutions to Eqs. (17) and (19) are possible. We still ignore the induced scalar potential A_0. The solutions, though not exact, can give us an idea about how they differ from the lowest-order ones and how they vary with g.

We solve for $A(r)$ and $j(r)$ satisfying Eqs. (17) and (19) using an iterative method initiated with the expressions in Eq. (8) for the induced current density. Results of convergent $r^2 j(r)$ are displayed in Fig. 2 for $F=0.9$ and $g=1$, 10, 14, respectively. We find that the curves do not monotonically decrease in r with respect to those derived from the lowest-order analysis. The variations can be interpreted in terms of the radius-dependent effective flux $F-grA(r)$. In the region of r where the applied flux F is reduced from 0.9 to 0.5 by the induced one, $r^2 j(r)$ grows with r. Afterward, it decreases and vanishes at large r, following the lowest-order curve corresponding to the net flux $F-gh$. These curves also show that the decrease becomes stronger with increasing g, and the induced current is distributed in a region characterized by $1/g$, as expected.

Results of convergent $grA(r)$ for the same values of F and g are exhibited in Fig. 3, where the dotted curves indicate the corresponding ones obtained from the model $A(r)$. They show a similar characteristic length scale $1/g$ again. Note that the difference between the two curves increases with g for $g<10$ and decreases afterward. The consistency of the model with the exact $grA(r)$ is already very good as g attains 14, so that we are convinced of the conclusions about the $g \to \infty$ behavior acquired from Eq. (22). The induced current densities derived from the model $A(r)$ also show the same degree of consistency to the numerical ones. We do not display them in Fig. 2 for simplicity.

The behavior of the induced charge density $\rho(r)$ is studied using Eq. (26) with the numerical solutions $A(r)$

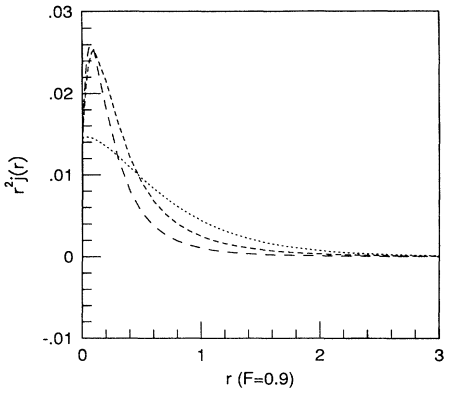

FIG. 2. The r dependence of the induced current density $r^2 j(r)$ for $F=0.9$, and $g=1$, 10, and 14, exhibited with the dotted, short-dashed, and long-dashed curves, respectively.

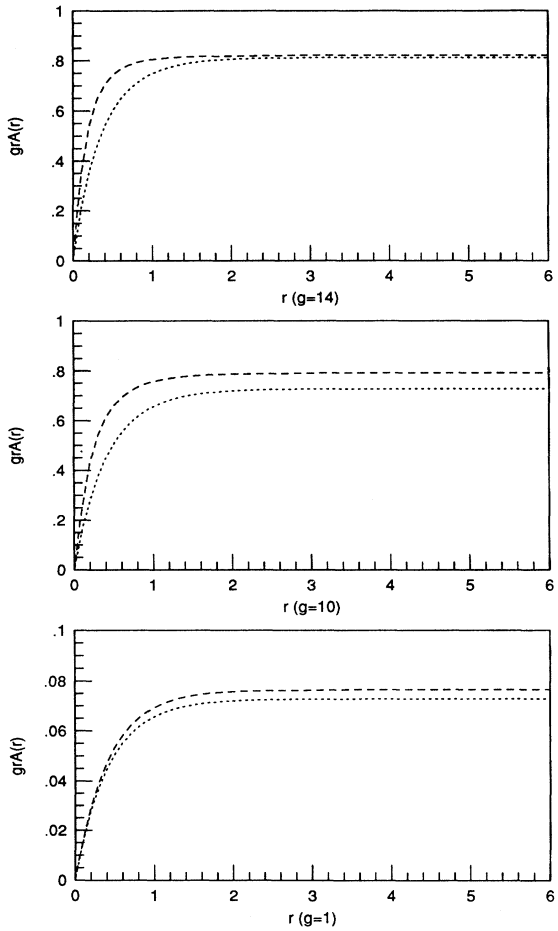

FIG. 3. The r dependence of the self-consistent induced vector potential and the model $grA(r)$ from Eq. (22), presented with the dashed and dotted curves, respectively, for $F=0.9$, and $g=1$, 10, and 14.

inserted, and results for $r\rho(r)$ are shown in Fig. 4. The curves possess similar features to those for $j(r)$.

We expect that the inclusion of A_0 will pull the vacuum currents toward the origin due to the attraction between opposite induced charges. However, the qualitative features mentioned above are maintained. At the same time, Q is reduced because of the more complete cancellation between opposite charges. Based on this argument, the effect of the induced scalar potential is less important. The neglect of A_0 is especially successful in the large-g limit since Q decreases as $1/g^{3/2}$ as explained in Sec. III.

In Sec. III we have absorbed the feedback effect due to the induced current into the index of the Bessel function. The purpose of this approximation is to maintain the symmetric cancellation employed in the lowest-order calculation so that we do not need to consider all partial waves. The solution matches the exact one very well for $g\rightarrow\infty$ because $rA(r)$ becomes constant for $r>0$ in this limit. For intermediate g, Eq. (18), obtained from the assumption that grA is constant, should be thought of as the leading term in a series expansion of the exact wave function in the derivative of grA. Therefore, we shall study how the results for intermediate g are modified by

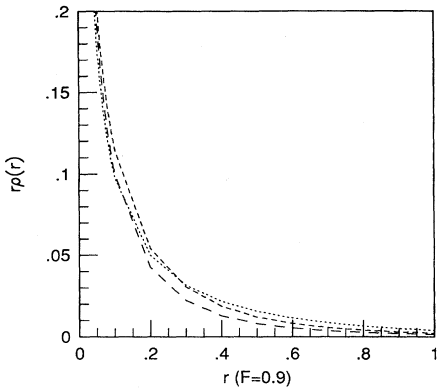

FIG. 4. The r dependence of the induced charge density $r\rho(r)$ for $F=1$, and $g=1$, 10, and 14, exhibited with the dotted, short-dashed, and long-dashed curves, respectively.

the contribution from the next-to-leading term. The expansion of the wave function to the first derivative of grA is derived by inserting Eq. (18) into the right-hand side of Eq. (15):

$$\begin{bmatrix}\chi_1\\ \chi_2\end{bmatrix}=\left[\frac{k}{4\pi}\frac{E+1}{E}\right]^{1/2}\begin{bmatrix} J_{q\nu'}+\frac{g}{k}\frac{d(rA)}{dr}\frac{dJ_{\bar\nu}}{d\bar\nu}\Big|_{\bar\nu=q(\nu'+1)} \\ \frac{iqk}{E+1}\left[J_{q(\nu'+1)}-\frac{g}{k}\frac{d(rA)}{dr}\frac{dJ_{\bar\nu}}{d\bar\nu}\Big|_{\bar\nu=q\nu'}\right]\end{bmatrix}, \tag{28}$$

where $\nu'\equiv\nu+grA$. Comparing Eq. (28) to (18), the correction Δ_ν to the νth term $(k^2/2\pi E)qJ_{q\nu'}J_{q(\nu'+1)}$ in the sum for the integrand of the induced current density from the first derivative of grA is given by

$$\Delta_\nu=-\frac{qkg}{4\pi E}\frac{d(rA)}{dr}\left[\frac{dJ_{\bar\nu}^2}{d\bar\nu}\Big|_{\bar\nu=q\nu'}-\frac{dJ_{\bar\nu}^2}{d\bar\nu}\Big|_{\bar\nu=q(\nu'+1)}\right]. \tag{29}$$

Summing Eq. (29) over all partial waves, a similar symmetric cancellation to that in the calculation for the induced charge density leads to

$$\sum_\nu\Delta_\nu=\frac{kg}{4\pi E}\frac{d(rA)}{dr}\frac{d}{d\bar\nu}(J_{-\bar\nu}^2-J_{\bar\nu}^2)\Big|_{\bar\nu=F-grA}. \tag{30}$$

Integrating Eq. (30) over k we obtain the correction to the induced current density:

$$\Delta j(r)=g\frac{d(rA)}{dr}\frac{d}{d\bar\nu}\rho_{\bar\nu}(r)\Big|_{\bar\nu=F-grA}, \tag{31}$$

where the induced charge density $\rho_{\bar\nu}$ is given by Eq. (26) with $F-grA$ replaced by $\bar\nu$.

Equation (31) is evaluated for $g=10$ with the numerical solution $A(r)$ inserted. Results for the modified induced current density $r^2(j+\Delta j)$ are exhibited in Fig. 5. Note that this correction is not self-consistent, but it shows the tendency of the modification. It is observed that the correction vanishes for $r>1$, where grA is essentially constant, and enhances the preliminary results in the region of small r, with the features of the curve maintained. A similar numerical evaluation has been carried out for $g=1$ and 14. For the former, the first-derivative correction is less obvious because of smaller $gd(rA)/dr$. For the latter, the deviation is of the same degree as that for $g=10$. We expect that a self-consistent analysis for the first-derivative correction will reduce the deviation. The approximate solutions Eq. (18) are thus reliable for intermediate g, at least qualitatively.

Based on the above formalism, the consistent solutions for $g\rightarrow\infty$ can be justified by examining the asymptotic behavior of the first-derivative contribution. We observe that, from the model $A(r)$, $\Delta j(r)$ is nonvanishing only in the range $r\sim 1/s^2\sim 1/g$, and its magnitude behaves like $\Delta j\sim gd(rA)/dr\sim ghs^2\sim g$ from Eq. (23), since the derivative of the charge density is finite. This correction to $j(r)$ gives rise to a corresponding $\Delta A(r)$ to $A(r)$. If ΔA vanishes faster than A as $g\rightarrow\infty$, the current density will not change, and the consistent solutions are stable. We find that, from Eq. (17), $r(\Delta A)\sim\Delta j r^3<1/g^2$, because $r\lesssim 1/g$. Compared to $rA\sim 1/g$, the correction is negligible.

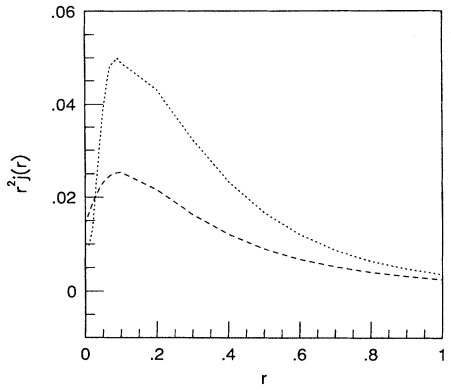

FIG. 5. The behavior of the induced current densities $r^2j(r)$ with and without the first-derivative correction from $grA(r)$, exhibited with the dotted and dashed curves, respectively.

V. CONCLUSION

In this paper we have explicitly calculated the self-consistent vacuum currents in the presence of a MFS in the limits $g \to 0$ and $g \to \infty$. Their decreasing features at large g, which are not shown in a lowest-order consideration, indicate that negative vacuum currents move toward the origin and cancel the positive ones. We have also demonstrated the transition of the characteristic length scale for the vacuum polarization from the fermion Compton wavelength at small g to the photon one at large g. Combining the observations in these two limits gives us an approximate picture for intermediate g. Compared to the case $g \to 0$, the vacuum currents are more compressed near the origin due to the smaller photon wavelength, and their magnitudes decrease faster because of the cancellation by the contribution from "infinity." These observations are justified by the explicit numerical analysis in Sec. IV.

It is shown in our results that no localized induced charge exists at the origin for $F \to 1$ when $g \to \infty$, since the cancellation is complete in that case. In fact, there should be no point induced charge for arbitrary g if we take into account the induced scalar potential, which gives a strong repulsion for an extremely concentrated charge density. Therefore all the induced quantities are distributed with an exponentially decaying tail. It is also shown that the system with fermion mass $m \to 0$ and fixed charge e coincides with that of massless fermions. The apparent difference between them disappears in an all-order analysis.

The approximations made in Sec. III are designed to study the $g \to \infty$ behavior, so we do not expect that they work equally well for arbitrary g. However, the modification from the first derivative of grA is still consistent with the expected behavior for intermediate $g \sim 10$ as shown in Sec. IV. Hence, the results give a rough description for the system. Higher-derivative corrections can be included systematically and analyzed self-consistently according to the formalism proposed in Sec. IV. Bound-state solutions will appear if we consider the induced scalar potential, but they do not change the features mentioned above very much. These bound states become weaker with increasing g because gA_0 decreases as $1/g^{1/2}$.

There is only a single dimensionless parameter $g = e^2/m$ in the analysis of $(2+1)$-dimensional QED. Therefore, the limit $g \to \infty$ can be equivalently understood as either $e \to \infty$ or $m \to 0$. At the same time, the radiative corrections from virtual photons, which become very massive in the large-g limit, are highly suppressed. The analysis with the quantum fluctuations excluded then turns out to be exact, that is, our quantum mechanical treatment is the same as QED. For intermediate g such quantum effects on the induced gauge field may become important. Since the total flux and angular momentum are conserved, knowing the exact behavior for $g \ll 1$ and $g \to \infty$ leads one to conclude that for intermediate g the modifications to the induced quantities from quantum fluctuations will preserve the qualitative results presented here. The method developed in this paper can also be applied to the similar system in $3+1$ dimensions [13]. Other induced quantities such as the induced angular momentum [10] might be a good check for our conclusions. Other approaches such as Schwinger's "proper-time" formalism [14,15] should lead to similar results. It might be worthwhile to investigate these topics in detail.

ACKNOWLEDGMENTS

We would like to thank J. M. Leinaas and R. R. Parwani for helpful discussions. This work was supported in part by the National Science Foundation under Grants Nos. NSF PHY-9108054 and NSF PHY-9107261.

[1] A. J. Niemi and G. W. Semenoff, Phys. Rev. Lett. **51**, 2077 (1983); Phys. Rep. **135**, 99 (1986).
[2] A. N. Redlich, Phys. Rev. Lett. **52**, 18 (1984); Phys. Rev. D **29**, 2366 (1984).
[3] Ph. de Sousa Gerbert, Phys. Rev. D **40**, 1346 (1989).
[4] P. Górnicki, Ann. Phys. (N.Y.) **202**, 271 (1990).
[5] R. R. Parwani and A. S. Goldhaber, Nucl. Phys. **B359**, 483 (1991).
[6] E. G. Flekkøy and J. M. Leinaas, Int. J. Mod. Phys. A **6**, 5327 (1991).
[7] S. Deser, R. Jackiw, S. Templeton, and J. Schonfeld, Phys. Rev. Lett. **48**, 975 (1982); Ann. Phys. (N.Y.) **140**, 2390 (1985).
[8] D. Boyanovsky, R. Blankenbecler, and R. Yahalom, Nucl. Phys. **B270**, 483 (1986).
[9] H. Banerjee, G. Bhattacharya, and J. S. Bhattacharyya, Phys. Rev. D **37**, 1706 (1988).
[10] M. B. Paranjape, Phys. Rev. Lett. **55**, 2390 (1985).

[11] H. Banerjee, G. Bhattacharya, and J. S. Bhattacharyya, Phys. Lett. B **189**, 431 (1987).
[12] S. Rao and R. Yahalom, Phys. Lett. B **172**, 227 (1986).
[13] H. N. Li, Academia Sinica Report No. IP-ASTP-15-92, 1992 (unpublished).
[14] J. Schwinger, Phys. Rev. **82**, 664 (1951).
[15] A. Chodos, D. A. Owen, and C. M. Sommerfield, Phys. Lett. B **212**, 491 (1988).